COMPUTATIONAL ANALYSIS OF PROGNOSIS OF MYOCARDIAL INFARCTION IN LEFT VENTRICLE

Md. Tofazzal Hossain[1*], Badhan Saha[2]
[1,2]*Department of Mechanical and Production Engineering,*
Ahsanullah University of Science and Technology, Dhaka 1208, Bangladesh

[*]Corresponding Author
E-mail Id: tofazzal.me@aust.edu

ABSTRACT

Heart Failure due to Acute Myocardial Infarction (HF AMI) has emerged as a prevalent heart disease with a high risk of short-term and long-term mortality rates. HF AMI has been associated with a progressively impaired interaction between the left ventricle (LV) and the systemic arteries. Because of the lower global transverse and longitudinal strain in AMI, it's been suggested that the LV's stiffness and contractility are compromised. Reduced ejection fraction (EF) and changes in LV geometry, such as infarct zone (IZ) size and location, as well as myocardial wall qualities such as contractility and stiffness, which may also alter global strains, support these results. To resolve these challenges, we used a proven mathematical comprehensive framework of a finite element LV model to separate the effects of AMI characteristics on systolic function measures. Simulations were done to assess the impact of changes in LV shape, and myocardial stiffness on cardiomyocyte strains. We found that the simultaneous increase in myocardial stiffness may mimic the systolic blood pressures, EF, and strains reported in AMI patients. These data imply that myocardial stiffness is enhanced in individuals with HF AMI.

Keywords: Acute Myocardial Infarction (AMI), Heart Failure, Myocardial Stiffness, Myocardial contractility, Finite Element modeling

Introduction

Thirty percent of the world's deaths are attributed to cardiovascular disease, the most prevalent cause of mortality worldwide. Coronary artery disease and stroke account for more than 75% of these deaths [1]. Tobacco use, being overweight, and having high cholesterol or blood pressure are all risk factors for heart disease.

These cardiovascular disorders might range from mild chest discomfort and shortness of breath to more severe chest pain and breathlessness. When diagnosing heart failure (HF), ejection fraction, or the proportion of blood expelled from the left ventricle (LV) with each pulse, is employed as a clinical indication to diagnose HF. Sudden blockage or cut-off of the blood supply is described as a "heart attack." It is possible that a MI may go unnoticed for an extended period or may lead to hemodynamic worsening and even death.

Many heart attacks are caused by coronary artery disease (CAD) - the common cause of mortality. When the coronary artery (CA) is completely blocked, the heart's myocardium is starved of oxygen and nutrients supply. MI and CAD are closely linked.

An international multicenter case-control study, INTERHEART, identified the

following modifiable CAD risk factors: depression, global stress, financial stress, and life events are all associated with an increased risk of cardiovascular disease and other chronic illnesses.

Except for excessive alcohol consumption, all of the above risk factors were significantly linked to an AMI in the INTERHEART study. Drugs, smoking, cold weather, and extreme stress trigger the progression of AMI. Infarction heals via tissue injury, heart dilatation, and cardiac dysfunction due to the myocardium's inability to regenerate [2].

Sweating, chest pain, upper extremity pain, and stomach discomfort can all be symptoms of AMI [3]. MI can appear in various ways, including palpitations and cardiac arrest. In addition, there are situations when the MI does not show any symptoms [4].

MI is a leading cause of premature death and morbidity in the world. Long-term heart failure risk is continuously high, despite improvements in early survival following ST-segment elevation MI (STEMI). LV systolic function, and in particular, LV ejection fraction (LVEF), is the standard of treatment for determining the first severity of heart damage [5].

However, global assessments of LV pump performance are unsophisticated compared to biomechanical characteristics such as myocardial contractility and stiffness. The main cause of death in the world is heart disease. Computer models simplify identifying the differences between a healthy and a diseased heart's mechanics. In recent decades, the realistic geometry and architectural structure of cardiac muscle fibers in FE models have advanced substantially.

According to the available literature, either an electrical circulatory system analog or a separate FE heart model was built and used with the FE model in either an open [6-8] or closed-loop [9]. The coupled electrical analog was constructed using a simplified description of the peripheral cardiac system based on a time-varying elastance function.

Pulsatile models [10] and outlet boundary restrictions are often employed in open-loop circulatory modelling frameworks to mimic blood ejection. Posterolateral or inferior LV wall myocardial infarction (MI) is distinct from anteroapical LV wall myocardial infarction (MI).

Preventing posterolateral MI from expanding and improving survival rates are the main benefits of this kind of MI. Posterolateral MI causes the posterior papillary muscle to migrate laterally, which causes persistent ischemic mitral regurgitation [11].

Sacks and Humphrey et al. [8] have published passive ventricular tissue biaxial mechanical testing findings for material qualities and mechanical analysis. Hunter and McCulloch's group published several key articles regarding how the structure of the ventricle's fibers affects its mechanical conditions.

Ultrasound elastic tensor imaging is equivalent to magnetic resonance diffusion tensor imaging in terms of fiber orientation. Using shear wave imaging, Lee et al. [12] attempted to measure the orientation of fibers in an open chest animal model. Shear wave imaging was used to evaluate changes in myocardial stiffness during the cardiac cycle. According to their research, big collagen fiber structure is a key factor in determining the mechanical characteristics of scars.

More recently, it was found that image-based cardiac mechanical models might be effective for clinical and surgical applications.

The passive mechanical characteristics of a porcine infarct were determined using MRI and finite element techniques. Peskin's famous first model with moving boundaries using an immersed-boundary method, the early MRI-based models for mechanical analysis, and investigations by Lee et al. [12] passive/active models, including the Continuity package, have all been developed to investigate cardiac mechanics with potential clinical applications.

The authors have developed patient-specific CMR-based RV/LV models with fluid-structure interactions (FSI) that may be used for various surgical designs and prospective applications. It has been shown that patients with MI have different morphology, mechanics, and biology than healthy volunteers.

Under four scenarios, Sack et al. [8] describe major recent advancements in the Living Heart Model (LHM) and utilize the LHM to compute left ventricular (LV) and right ventricular (RV) myofiber stress distributions.

Acute left heart failure (ALHF) treated with an LV assist device flow rate of 2 L/min. ALHF was treated with an LV assist device flow rate of 4.5 L/min for ALHF. Four sheep with LV infarcts and six sheep with infarcts repaired surgically were studied by Walker and colleagues.

They used cardiac catheterization, three-dimensional MRI with tissue tagging, MR diffusion tensor imaging, and an advanced FE method (explicitly developed for cardiac mechanics to measure regional systolic myocardial material properties in the beating hearts of these animals. But even though both prior types of research represent breakthroughs, they both used a manually led pseudo-optimization.

On the other hand, Wenk et al. [13] employed mathematical models of infarcted LV to define and quantify its regional contractility. On the other hand, these models assume that the contractility in the BZ, distant, and infarct areas is homogenous. This results in a sudden shift in contractility at infarction–BZ and remote borders.

In this research, finite element modelling (FEM) has been used to explore the impact of myocardial infarction on the function of the left ventricle (LV). It has become more common for people with heart disease to suffer from severe MI. The underlying cause of acute MI remains a mystery due to a lack of adequate clinical studies and research resources.

To the best of our knowledge, very few studies using finite element modeling have been conducted on MI in the past. In our study, we have focused on finding out the effects of infarct size and location by changing the contractility and other relevant model parameters, which directly influence the overall function of the LV.

METHODS
MODELLING THE SYSTEMIC CIRCULATORY SYSTEM
A closed-loop lumped parameter circulatory model was used for the systemic circulatory system, with other systemic circulatory compartments coupled to the LV finite element model.
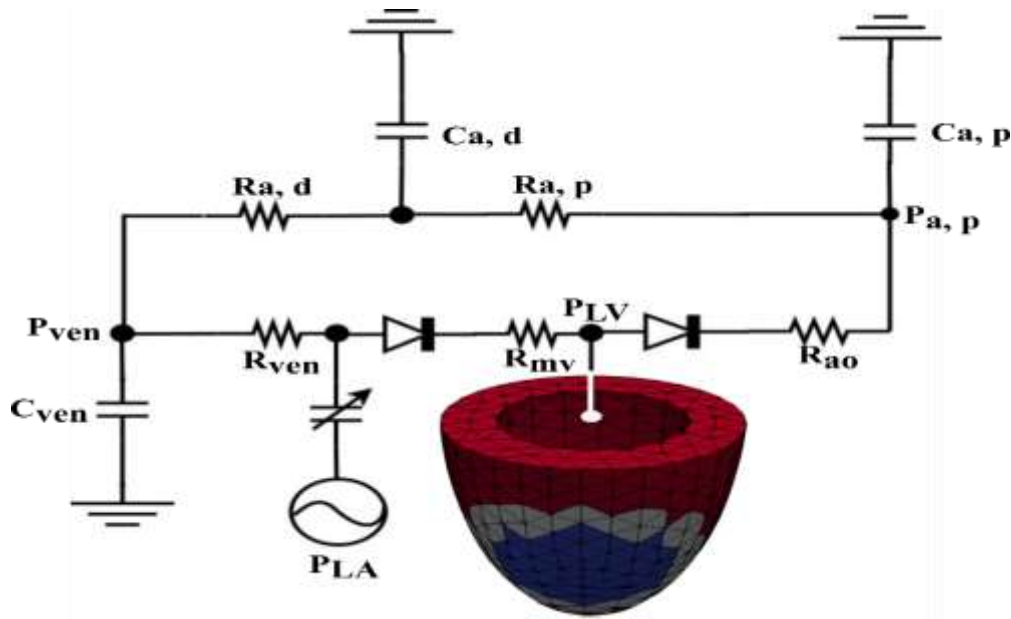
Fig. 1 *Schematic diagram of the modeling framework showing the LV FE model and other compartments of the systemic circulation which were modeled using their electrical analog [12].*

To connect finite element models of the LV, a closed-loop modeling technique for the systemic circulation circuit was used. The other circuit components were modeled using electrical analogies (**Fig. 1**). Since the entire mass of blood in the circulatory system has to be preserved, the rate of volume change in each storage compartment of the circulatory system must be coupled to the net change in inflow and outflow rates by the following equations (Eq. 1-4) [12]

$$\frac{dV_{LV}(t)}{dt} = q_{mv}(t) - q_{ao}(t) \tag{1}$$

$$\frac{dV_{a,d}(t)}{dt} = q_{a,p}(t) - q_{a,d}(t) \tag{2}$$

$$\frac{dV_{LA}(t)}{dt} = q_{ven}(t) - q_{mv}(t) \tag{3}$$

$$\frac{dV_{ven}(t)}{dt} = q_{a,d}(t) - q_{ven}(t) \tag{4}$$

$$\frac{dV_{a,p}(t)}{dt} = q_{ao}(t) - q_{a,p}(t) \tag{5}$$

Where, q_{mv}, $q_{a,p}$, q_{ao}, q_{ven}, and $q_{a,d}$ are volumetric flow rates at various segments, whereas V_{LV}, $V_{a,d}$, V_{LA}, V_{ven}, and $V_{a,p}$ are volumes of the LV, distal artery, LA, vein, and proximal artery, respectively. The flow resistances of the respective components (R_{ven}, $R_{a,p}$, $R_{a,d}$, R_{ao}, and R_{mv}) and the pressure drop between neighboring compartments determine the volumetric flow rates of distinct components of the circuit. The flow rates are calculated based on the following equations (Eq. 6-10) [12].

The constant volumes at the rest of the veins, proximal, and distal arteries are $V_{ven,\,0}$, $V_{ap,\,0}$, and $V_{ad,\,0}$, respectively. The total passive stiffness of the veins, proximal, and distal arteries is represented by C_{ven}, $C_{a,\,p}$, and $C_{a,\,d}$, respectively.

However, the following equations (Eq. 6-9) [12], which use a time-varying elastance function to describe the contraction of the left atrial, required that pressure in the left atrium $P_{LA}(t)$ be a function of its volume $V_{LA}(t)$.

$$P_{LA}(t) = e(t)P_{es,LA}(V_{LA}(t)) + (1 - e(t))P_{ed,LA}(V_{LA}(t)) \tag{6}$$

where,

$$P_{es,LA}(V_{LA}(t)) = E_{es,LA}\big(V_{LA}(t) - V_{0,LA}\big) \tag{7}$$

$$P_{ed,LA}(V_{LA}(t)) = A_{LA}\big(e^{B_{LA}(V_{LA}(t) - V_{0,LA})} - 1\big) \tag{8}$$

And,

$$e(t) = \begin{cases} \dfrac{1}{2}\left(\sin\left[\left(\dfrac{\pi}{t_{\max}}\right)t - \dfrac{\pi}{2}\right] + 1\right); & 0 < t \le 3/2\,t_{\max} \\ \dfrac{1}{2}e^{-(t - 3/2\,t_{\max})/\tau_{LA}}; & t > 3/2\,t_{\max} \end{cases} \tag{9}$$

In Eq. (7-8), $V_{0,\,LA}$ is the volume axis intercept of the end-systolic pressure-volume relationship (ESPVR), A_{LA} and B_{LA} are parameters of the left atrium's end-diastolic pressure-volume relationship (EDPVR), and $E_{es,\,LA}$ is the end-systolic elastance. Eq. (9) gives the driving function $e(t)$, where τ is the relaxation time constant and t_{max} is the maximum chamber elastance point. **Table 1** shows the values of $E_{es,\,LA}$, $V_{0,\,LA}$, A_{LA}, B_{LA}, t_{max}, and τ_{LA}.

Table 1 Time-varying elastance model parameters for left atrium [12].

Parameters	Units	Values (Normal and AMI heart LV baseline)
End-systolic elastance, $E_{es,LA}$	Pa/ml	60
Scaling factor for EDPVR, A_{LA}	Pa	58.67
Time constant of relaxation, τ	ms	25
Exponent for EDPVR, B_{LA}	ml^{-1}	0.05
Time to end-systole, t_{max}	ms	120
Volume axis intercept, $V_{0,LA}$	ml	10

Furthermore, the LV pressure is a function of its corresponding volume that can be correlated by a non-closed form function as shown in Eq. (10) [12],

$$P_{LV}(t) = f^{LV}(V_{LV}(t)) \tag{10}$$

The functional relationship between LV pressure and volume was determined using the FE approach, as explained below. The parameter values for the closed-loop circulatory model are listed in **Table 2**.

Table 2 Fixed values of the model parameters for all simulation cases.

Parameter	Unit	Values
Aortic valve resistance, R_{ao}	Pa ms ml^{-1}	500
Proximal aorta resistance, $R_{a, p}$	Pa ms ml^{-1}	18000
Venous resistance, R_{ven}	Pa ms ml^{-1}	100
Mitral valve resistance, R_{mv}	Pa ms ml^{-1}	200
Proximal aorta compliance, $C_{a, p}$	ml Pa	0.0032
Distal aorta compliance, $C_{a, d}$	ml Pa	0.033
Venous compliance, C_{ven}	ml Pa	0.28
Resting volume for proximal aorta, $V_{ap, 0}$	ml	360
Resting volume for distal aorta, $V_{ad, 0}$	ml	40

LV GEOMETRY, MESHING, AND MICROSTRUCTURE OF THE LV

A normal person and a patient with acute myocardial infarction (AMI) were studied in Singapore's National Heart Center (NHC) to gather clinical data and MR images of the left ventricle. Endocardium surfaces were created based on the MR scans of a normal patient and an AMI patient (**Fig. 2**). Based on the reconstructed LV endocardium surfaces, the 3D LV geometry was built using a half prolate ellipsoid shape. As determined by the clinical data, the LV volume was designed to reflect the minimal pressure state, which lies somewhere between the normal range of ESV and EDV, but close to EDV. **Table 3** shows the LV models' geometrical parameters. Based on earlier studies [14], the wall thickness of the LV has been modified here.
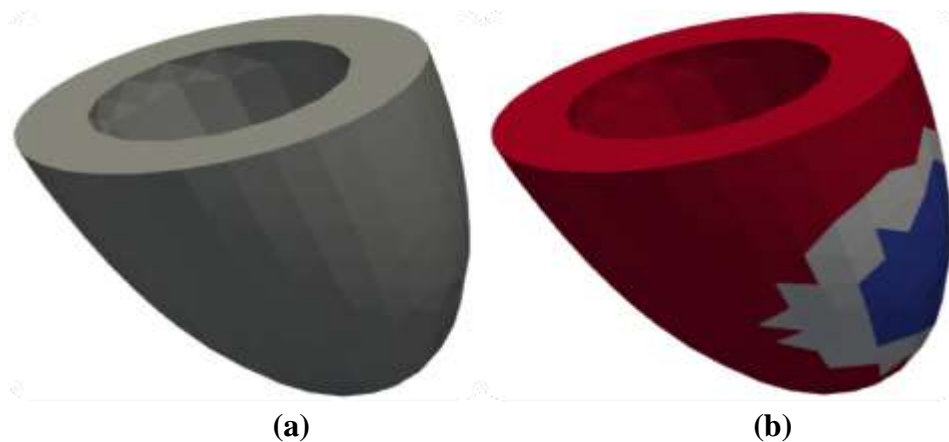

(a) **(b)**
Fig. 2 Half prolate ellipsoid geometrical models of LV, constructed based on the acquired MRI images of (a) normal subject and (b) AMI patient.

Table 3 Geometrical Parameters of LV for Normal and AMI baseline model.

	Normal (healthy) heart LV	AMI heart LV
Cavity Diameter (cm) (at basal plane)	4.00	4.00
Length, L (cm)	8.30	8.30
Wall thickness, WT (cm)	1.13	1.13

The discretized LV geometry with 1150 - 1600 quadratic tetrahedral components was created to perform the grid independence test and is depicted in **Fig. 3**. Each quadratic element had a total of ten nodes, each of which had three degrees of freedom (DOF) and could be rotated in three Cartesian coordinate directions. As a result, each quadratic element has a total of 30 degrees of freedom. The myocardial fibers of the left ventricle are organized helically over the length of the ventricle (**Fig. 4**). A linear transmural variation was used to vary the helix angle associated with myofiber orientation, which ranged from 60° at the endocardium to -60 ° at the epicardium in the left ventricular (LV) based on existing literature data [15] (**Fig. 4**). Because every fiber in the myocardium is intricately intertwined, deformation occurs as a result of the combined efforts of all the fibers. There are only two types of LV deformation metrics that can be used: (i) three orthogonal components of myocardial deformation (longitudinal shortening, circumferential shortening, and radial thickening), (ii) LV twist (circumferential–longitudinal shear strain resulting from the obliquely arranged double-helical orientation of LV myocardial architecture that greatly enhances the ability to pump blood). The obliquely oriented double-helical orientation of the LV myocardial architecture results in LV twist, which reflects circumferential–longitudinal shear strain and considerably enhances LV ejection (**Fig. 5**) [14].
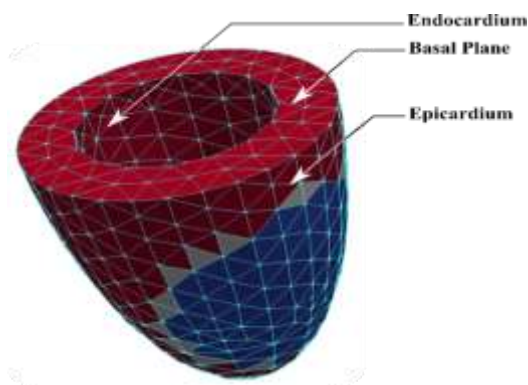

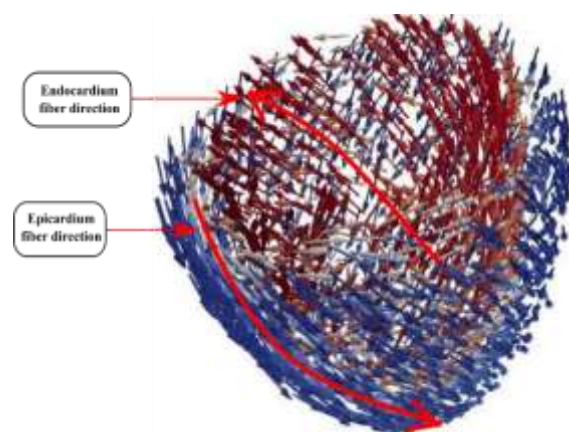*Fig. 3 LV geometry defined using a half prolate ellipsoid and discretized with quadratic tetrahedral elements*

Fig. 4 Myofiber path variation by helix angle from the LV endocardium to epicardium in the FE model.
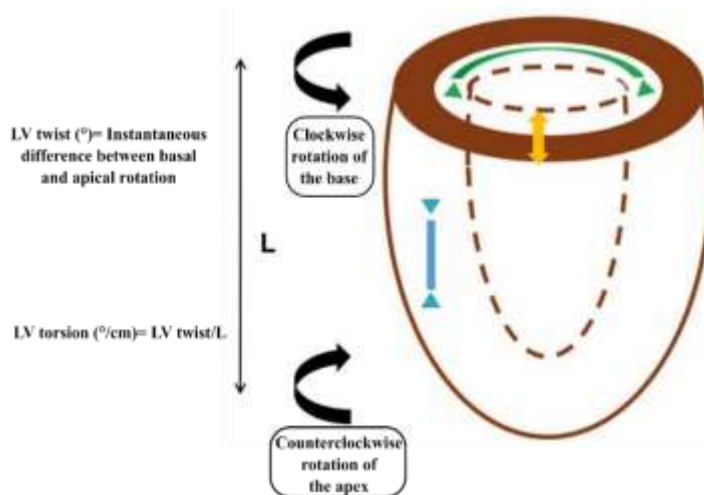
Fig. 5 *The three orthogonal planes of myocardial deformation are longitudinal shrinking (blue), radial stiffening (orange), and circumferential shortening (white) (green) under systolic conditions [15].*

GRID INDEPENDENCE TEST

A grid independence test was done to ensure that the finite element results were consistent with the fluctuation of the number of elements. 350 to 1830 quadratic tetrahedral elements have been run for a baseline case. **Fig. 6** depicts the PV loop, LV volume, and pressure waveforms for a typical LV model with different number of quadratic tetrahedral elements. The

maximum pressure difference between 1558 and 1830 elements cases is only ~1.88%. Also, the change in stroke volume between the two cases is about ~4.62%. As a result, approximately 1600 elements were selected for the numerical simulation of the various cases in this study to efficiently simulate the cases in terms of simulation time.
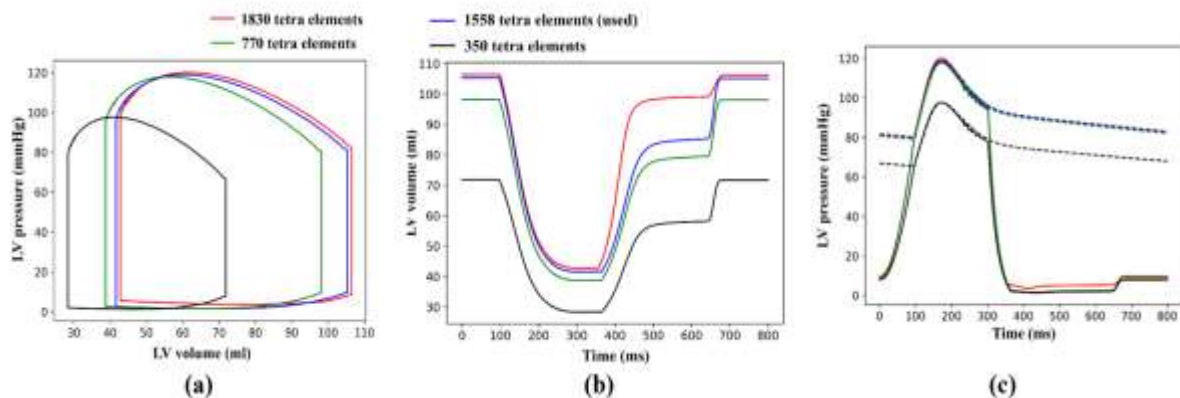

Fig. 6 *Comparison of (a) PV loop, (b) volume waveforms, and (c) pressure waveforms for the different number of elements.*

RESULTS AND DISCUSSION

The model was calibrated using data obtained from the clinical studies [16-17] to simulate a healthy subject and an infarct patient (AMI model). With these two models, the model's ability to accurately

predict patient-specific characteristics has been demonstrated. Following this, the calibrated AMI model was used to investigate various possible paths of progression by altering relevant parameters. Depending on the type of

geometry (infarct size and infarct location), the model parameters for contractility and stiffness were altered. These AMI models with isolated changes in geometry, contractility, or stiffness were compared to the healthy baseline model's results (hemodynamics and overall mechanical behaviors).

VALIDATION OF THE MODELS: NORMAL AND AMI CASE
COMPARISON BETWEEN THE MODEL AND CLINICAL DATA FOR THE HEALTHY SUBJECT

The PV loops, pressure, and volume waveforms of the LV for the normal subject predicted by the model were closely matched with the clinical data [14], as shown in **Fig. 7**. The reference EDV (~114 ml) and ESV (~45 ml) were reasonably matched with the model (~109 ml EDV and 43 ml ESV) (**Fig. 7 (a)**). As a result, the EF was 61% for the model, which is close to the reference EF of 65% [14] (which is within the normal EF range > 55%) [18]. Pressure waveforms of the LV as shown in **Fig. 7 (b)** in the baseline case also showed good agreement with the clinical data. The model aortic pressure waveform is within the normal range (systolic < 120 mmHg, diastolic < 80) with an aortic pulse pressure of 40 mmHg (systolic: 120 mmHg, diastolic: 80 mmHg). **Fig. 7 (b)** shows that both the model and data represent an approximately equal response for the contraction during the systole and relaxation during the diastole over the cardiac cycle. The outcomes of the normal case have been summarized in **Table 4**.

Table 4 Final outcomes of healthy LV model case

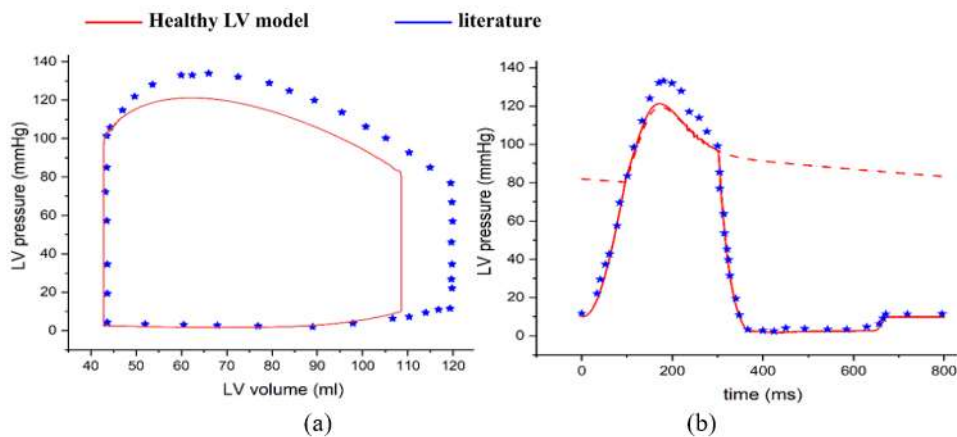| Outcome indices	Unit	Value
End-diastolic volume	ml	109
End-systolic volume	ml	43
Ejection Fraction, EF	%	61
End-systolic pressure, ESP	mmHg	121
End-diastolic pressure, EDP	mmHg	80

Fig. 7 *Comparison between the model prediction and clinical data [14] for LV (a) PV loop, and (b) pressure waveforms for the normal subject.*

COMPARISON BETWEEN THE MODEL AND CLINICAL DATA FOR THE AMI PATIENT

Similar to the healthy case, the PV loops, pressure, and volume waveforms of the LV for the infarct case (infarct size of ~9% of total LV volume, and the location of infarct at -4.5 cm from the basal plane) - with increased myofiber stiffness of 135 kPa and reduced myofiber contractility of 91 ms - predicted by the model was reasonably matched with the clinical data [16] as shown in **Fig. 8**. The reference EDV (83 ml) and ESV (39.5 ml) were reasonably matched with the model (83 ml EDV and 40 ml ESV) (**Fig. 8 (a)**). As a result, the EF was 52% for the model, which is close to the reference EF of 52.5% (within the heart failure range < 55% [18]). Pressure waveforms of the LV as shown in **Fig. 8 (b)** in the baseline AMI case also showed good agreements with the clinical AMI data. Similar to the healthy case, the contraction and relaxation phases during the systole and diastole respectively for the AMI model matched well with the clinical data. All the parameters were kept constant except the myofiber stiffness and contractility of the AMI LV model to investigate the effects of infarct zone properties. The changes in myofiber stiffness and contractility in the AMI LV model in comparison to the healthy LV model have been tabulated in **Table 5**.
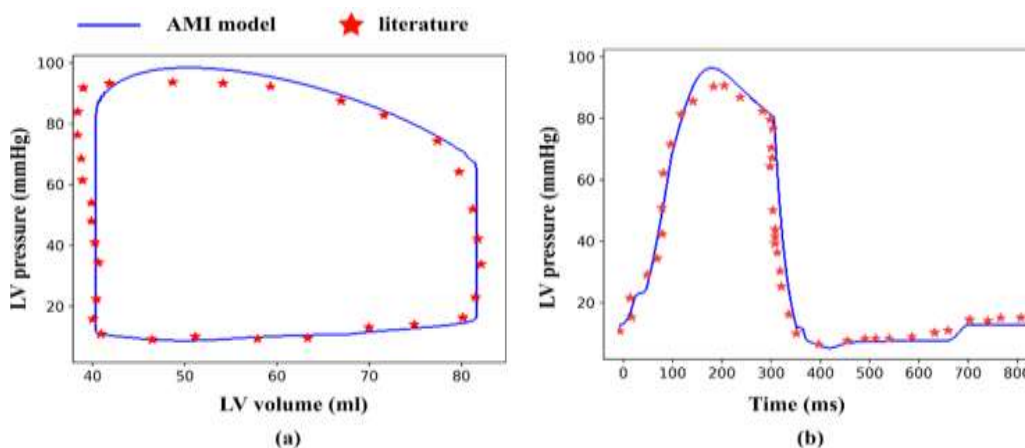

Fig. 8 *Comparison between the model prediction and clinical data [16] for LV (a) PV loop, and (b) pressure waveforms for the AMI patient.*

Table 5 *Variations in the model parameters of AMI LV in comparison to healthy LV*

Parameters	Healthy LV	AMI LV	% Change in AMI LV
Stiffness, C (kPa)	125	135	8% ↑
Contractility, Tmax (ms)	130	91	30% ↓
IZ location, z (cm)	-	-4.5	-
IZ radius, r_iz (cm)	-	2.75	-

EFFECTS OF INFARCT SIZE VARIATIONS IN AMI PATIENT

Managing patients with an acute ST-segment elevation myocardial infarction (MI) necessitates effective risk stratification. In previous studies, acute anterior MI patients had a worse prognosis than non-anterior MI patients because of more pronounced adverse left ventricular (LV) remodeling. As a result, risk assessment algorithms for the prognosis prediction of patients after acute ST-segment elevation MI have included the

anterior location of the MI. However, it is still unclear if the worse post-infarction LV remodeling and prognosis associated with anterior MI is due to greater MI size or if infarct location exerts a role further than MI size. This is a question that needs to be answered [19]. In this modeling study, both the variations have been studied. The rigidity or stiffness of the LV myofiber changes with the introduction of an infarct, and this rigidity or stiffness dramatically increases with the size of the infarct. The geometrical parameters of infarct size that are varied for different cases are tabulated in **Table 6**.

Table 6 Geometrical variations to study the effect of infarct size in AMI patients.

Case ID	Left ventricle volume, LVV (cm^3)	IZ volume, cm^3 (% LVV)	BZ volume, cm^3 (% LVV)	RZ volume, cm^3 (% LVV)	Infarct radius, r_iz (cm)	Infarct location, Z (cm)
Healthy: base		-	-	-	-	-
IZ size-1		9.50 (9%)	13.69 (13%)	82.12 (78%)	2.75	-4.5
IZ size-2	105.28	18.95 (18%)	8.42 (8%)	77.91 (74%)	3.25	-4.5
IZ size-3		28.43 (27%)	3.16 (3%)	73.70 (70%)	3.75	-4.5

PV loop, volume waveforms, and pressure waveforms for different infarct sizes are shown in **Fig. 9 (A)**, **Fig. 9 (B)**, and **Fig. 9 (C),** respectively. It can be observed from PV loops that both EDV and ESV of LV have decreased with the increased size of the infarct zone. It is seen from **Fig. 9 (A)** that for the infarct size of 9% (blue), 18% (green), and 27% (black) of LV volume, the EDVs have decreased to 83 ml, 66 ml, and 52 ml respectively from 109 ml EDV of the healthy case (red). And the corresponding ESVs are 40 ml, 35 ml, and 30 ml rather than the healthy ESV of 43 ml.

It is also noticeable that the corresponding ejection fractions (EF) of the cases have decreased consequently to 52%, 47%, and 43% from the healthy case's EF of 61%. For the increased size of the infarct, the contractility of the LV has decreased, while the rate of myocardial relaxation has increased.

The variations of circumferential strain (Ecc), longitudinal strain (Ell), and radial strain (Err) waveforms with the infarct size are shown in **Fig. 9 (D)**, **Fig. 9 (E)**, and **Fig. 9 (F),** respectively. The significant findings from these figures are that the changes in Ecc, Ell, and Err are in decreasing order with increasing infarct size. The absolute peak Ecc are 17%, 14%, and 8% for the infarct size of 9%, 18%, and 27%, respectively, whether it is ~24% for a healthy heart (**Fig. 9 (D)**).

The absolute peak Ell is 19%, 16%, and 14% (**Fig. 9 (E)**), and the absolute peak Err is 20%, 16%, and 12% (**Fig. 9 (F))**, for the infarct size of 9%, 18%, and 27% respectively, whether for healthy case the peak Ell and Err are 22% and 26%, respectively. The reduction in peak strains is consistent with the insights of the infarct size effects on the pressure-volume relations as the remodeling LV becomes stiffer with the scar formation, thrombus

effects, or increased hemodynamic loading status caused by myocardial infarction. The outcomes of pressure, volume, Ecc, Ell, and Err variations due to the infarct size are tabulated in **Table 7.**
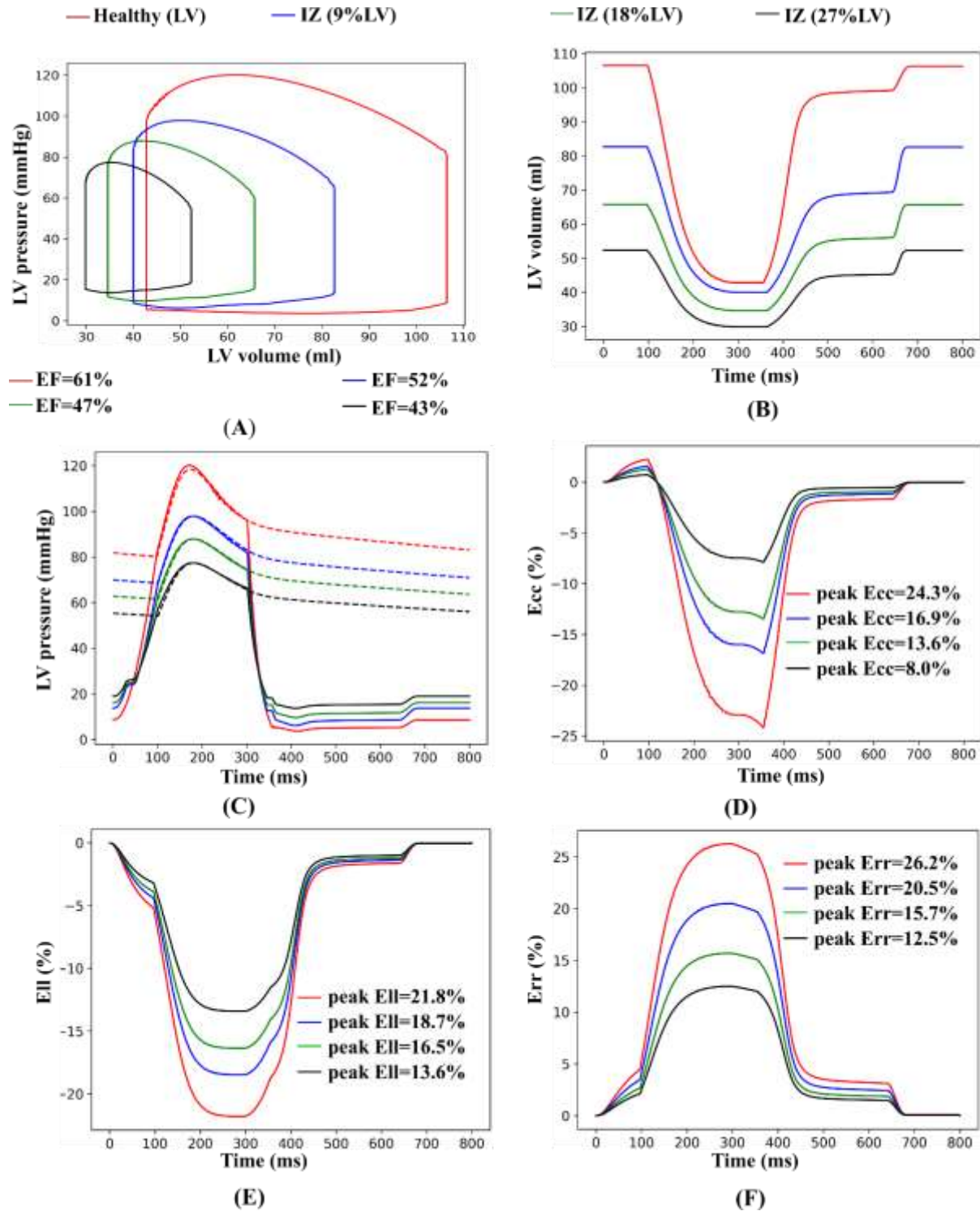

Fig. 9 Comparison among LV (A) PV loops, (B) volume waveforms, (C) pressure waveforms, (D) circumferential strains, (E) longitudinal strains, and (F) radial strains at different infarct zone size

Table 7 Model prediction of different LV functional indices for AMI cases with different sizes of infarct zone.

	Healthy LV [14]	Infarct Size [20]			Clinical Range
		9% LVV	18% LVV	27% LVV	
End-diastolic volume, EDV (ml)	109	83	66	52	84.1-121.8 [20]
End-systolic volume, ESV (ml)	43	40	35	30	36.7-69.6 [20]
Ejection fraction, EF (%)	61	52	47	43	49.6±7.5 [20]
End-diastolic pressure, EDP (mmHg)	15	18	18.5	20	11.9±4.6 [21]
End-systolic pressure, ESP (mmHg)	100	90	80	70	99±5 [21]
Absolute peak Ecc (%)	24	17	14	8	13.45±4.1 [20]
Absolute peak Ell (%)	22	19	15	12	20±2.1 [20]
Absolute peak Err (%)	26	20	16	12	14±6 [20]

EFFECTS OF STIFFNESS CHANGE OF INFARCT ZONE IN BASELINE AMI PATIENT ON LV HEMODYNAMICS

Myocardial stiffness is believed to be a critical factor in initiating detrimental heart disease [22-23].

After myocardial infarction, ventricular remodeling increases mortality and is strongly linked with the amount of infarct transmurality. Infarct stiffness is predicted to impact regional mechanics and thus the likelihood of human ventricular remodeling. This, however, has not been thoroughly researched [24].

The purpose of this work is to examine the impact of infarct stiffness on myofiber regional mechanics using models from an actively contracting left ventricle. Calculating the appropriate amount of infarct stiffness is necessary to establish balanced regional mechanics across the cardiac cycle, which may be beneficial in therapy, such as myocardial hydrogel injection to regulate its stiffness and lower stress to prevent ventricular remodeling [24. This case of stiffness change has been performed using the AMI geometry model with 9% of infarct volume (case: IZ size1), and infarct location of z = -4.5 cm (case: IZ Location1). The parameters varied in this experiment are tabulated in **Table 8**.

It is seen from **Fig. 10 (A)** that the EDV has been decreased to 62 ml (IZ_C3 case: black) from 109 ml EDV of healthy LV (red). And the corresponding ESV is 34 ml, while for healthy LV, the ESV is 43 ml.

The EF has also decreased due to the increasing IZ stiffness. For the extreme case of stiffness (IZ_C3 case), the lowest EF was achieved, and it is 44% for this case reduced from 61% EF of healthy.

It can be said from **Fig. 10 (C)** that the peak LV pressure for the case of IZ_C3 is higher than the peak pressure of infarct size case of 27% (IZ size-3) (**Fig. 10 (C)**)), from where it is clear that the effects of stiffness are less than the effects of infarct size on the LV pressure. These findings are consistent with the results investigated by C. Leong et al. [23].

Table 8 Variations in stiffness parameter to investigate the effects in AMI patients.

Case ID	Stiffness, C_para (Pa)		
	Remote zone (RZ)	Infarct zone (IZ)	
	C (Pa)	C (Pa)	% Increase compares to remote zone (unaffected)
Healthy: base (C)	125	125	0
IZ_C1	125	135	8
IZ_C2	125	145	16
IZ_C3	125	155	24

The absolute peak Ecc for the stiffness cases of IZ_C1, IZ_C2, and IZ_C3 are 17%, 15%, and 11%, respectively, whereas the healthy heart has a peak Ecc of 24% (**Fig. 10 (D)**). For the cases, the absolute peak Ell is 19%, 15%, and 12% (**Fig. 10 (E)**), and the absolute peak Err is 20%, 18%, and 16% (**Fig. 10 (F)**), whereas the peak Ell and Err are 22% and 26% for healthy patients, respectively.

The findings of the stiffness change effects on strains are consistent with the pressure-volume relationships as the remodeling LV stiffens due to myocardial dysfunction and increased hemodynamic loading status, which promotes the stiffness of the infarct zone.

For the 20% increase in infarct zone stiffness, the absolute peak Ecc has been reduced by 54%, absolute peak Ell by 45%, and absolute peak Err by 38% in comparison to the healthy LV. The outcomes of pressure, volume, Ecc, Ell, and Err variations due to the change in infarct zone stiffness are tabulated in **Table 9**.
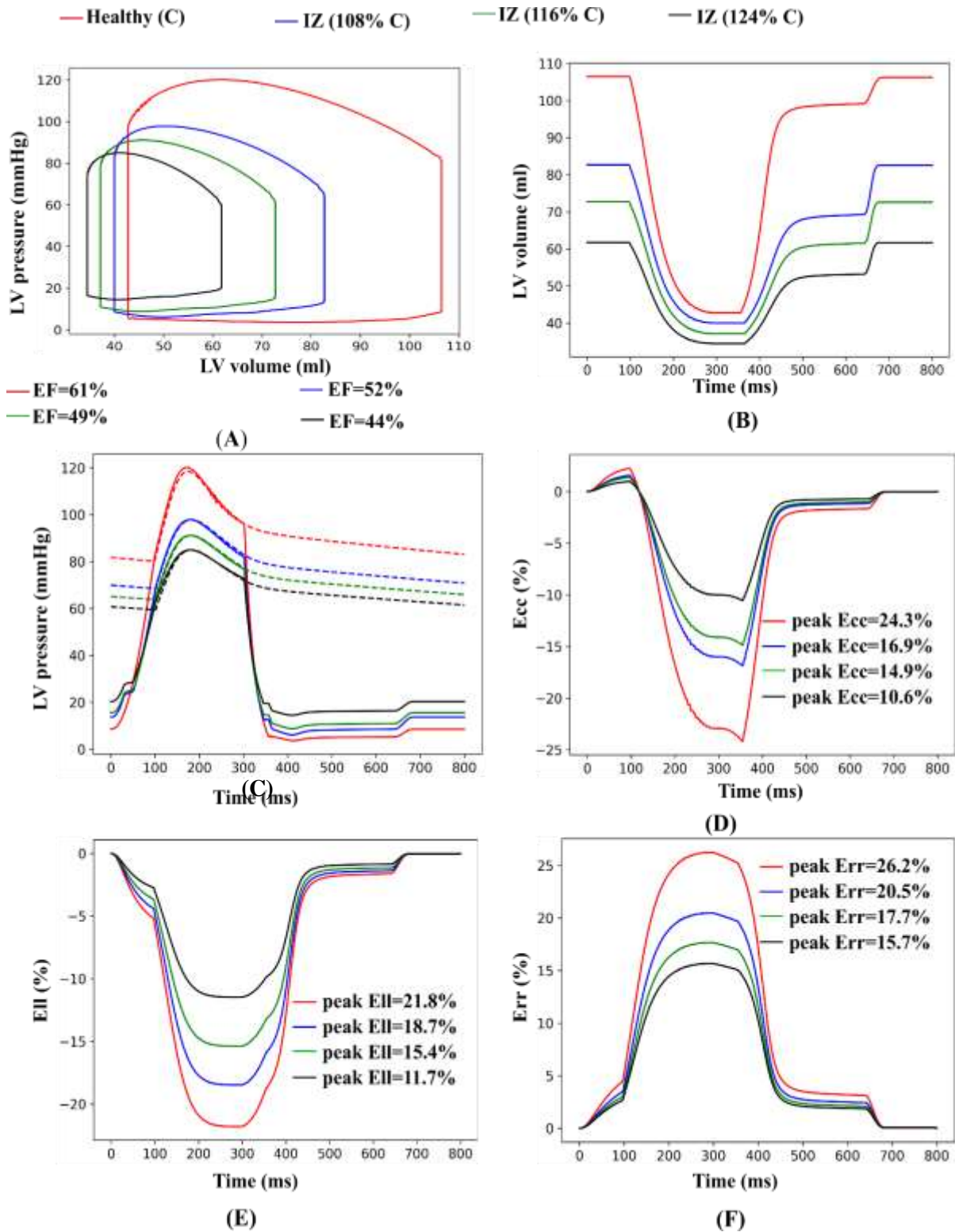
Fig. 10 Comparison among LV (A) PV loops, (B) volume waveforms, (C) pressure waveforms, (D) circumferential strains, (E) longitudinal strains, and (F) radial strains at different infarct zone stiffness (C parameter)

HBRP PUBLICATION

***Table 9** Outcome parameters of LV of both AMI and healthy model for different stiffness of infarct zone.*

	Healthy LV [14]	Infarct zone stiffness			Clinical Range
	125 Pa	135 Pa	145 Pa	155 Pa	
End-diastolic volume, EDV (ml)	109	83	73	62	84.1-121.8 [20]
End-systolic volume, ESV (ml)	43	40	37	34	36.7-69.6 [20]
Ejection fraction, EF (%)	61	52	50	44	49.6±7.5 [20]
End-diastolic pressure, EDP (mmHg)	15	18	18	20	11.9±4.6 [21]
End-systolic pressure, ESP (mmHg)	100	90	85	78	99±5 [21]
Absolute peak Ecc (%)	24	17	14	11	13.45±4.1 [20]
Absolute peak Ell (%)	22	19	15	12	20±2.1 [20]
Absolute peak Err (%)	26	20	18	16	14±6 [20]

SUMMARY AND CONCLUSION

In this research, a coupled LV FE-lumped parameter circulatory modeling framework has been developed to model acute myocardial infarction (AMI) patients. The baseline AMI model was successfully matched with the clinical data from the literature by calibrating the different model parameters.

The calibrated AMI model was used to study the effects of infarct size, and myocardial stiffness on the left ventricular function. It is found that the increase in the infarct size adversely affects the left ventricular function and gradually progresses towards more acute heart failure (HF). Increased infarct size means less active zone of LV, therefore, the LV function as indexed by EF gradually decreases. In addition, the peak longitudinal and circumferential strains decreased with the increase in infarct size. However, the decrease of peak circumferential strain was more severe than the longitudinal strain which suggests that the LV's ability of circumferential shortening was more severely affected than the longitudinal shrinking.

On the other hand, for particular infarct size, if the myocardial stiffness is increased then it has been found that for the 30% increase in myocardial stiffness the EDV, and ESV have been reduced by 43%, and 21% respectively, and the corresponding EF has been decreased by 28% which is approximately equal to the effects of the increased infarct size of 27% LVV (EF decreased by 29%).

Therefore, it can be concluded that myocardial stiffness can play a vital key in the forecasting of MI progression. And,

this model can be utilized in clinical studies with further incorporation of significant clinical data to improve the reliability of this model prediction.

CONFLICTS OF INTEREST:
The author declares the confirmation of having no conflict of interest concerning this work.

NOMENCLATURE

HF	: Heart Failure
EF	: Ejection Fraction
HFrEF	: Heart Failure with reduced Ejection Fraction
HFpEF	: Heart Failure with preserved Ejection Fraction
ED	: End Diastole
ES	: End Systole
LV	: Left Ventricle
LA	: Left Atrium
RV	: Right Ventricle
RA	: Right Atrium
SL	: Semilunar Valve
HTN	: Hypertension
DD	: Diastolic Dysfunction
AV	: Atrioventricular Valve
SV	: Stroke Volume
MR	: Magnetic Resonance
ECG	: Electrocardiography
DBP	: Diastolic Blood Pressure
SBP	: Systolic Blood Pressure
ESPVR	: End-Systolic Pressure-Volume Relationship
EDPVR	: End-Diastolic Pressure-Volume Relationship
TPR	: Total Peripheral Resistance
Ees	: End Systolic Elastance

REFERENCES

1. Virani, S. S. *et al.,* "*Heart disease and stroke statistics—2020 update: A report from the American Heart Association*." *Circulation* (2020). doi:10.1161/CIR.0000000000000757.

2. Frangogiannis, N. G., "Pathophysiology of myocardial infarction." *Compr. Physiol.* 5, 1841–1875 (2015).

3. Thygesen, K. *et al.,* "Fourth universal definition of myocardial infarction (2018)." *Kardiol. Pol.* 76, 1383–1415 (2018).

4. Thygesen, K. *et al.,* "Third universal definition of myocardial infarction." *Eur. Heart J.* 33, 2551–2567 (2012).

5. Gao, H. *et al.,* "Changes and classification in myocardial contractile function in the left ventricle following acute myocardial infarction." *J. R. Soc. Interface* 14, (2017).

6. Usyk, T. P., LeGrice, I. J. & McCulloch, A. D., "Computational model of three-dimensional cardiac electromechanics." *Comput. Vis. Sci.* 4, 249–257 (2002).

7. Shimkunas, R. *et al.,* "Left ventricular myocardial contractility is depressed in the borderzone after posterolateral myocardial infarction." *Ann. Thorac. Surg.* 95, 1619–1625 (2013).

8. Kevin L. Sack1, Brian Baillargeon2, Gabriel Acevedo-Bolton3, Martin Genet3, 4, 5, N., Rebelo2, Ellen Kuhl6, Liviu Klein7, Georg M. Weiselthaler3, Daniel Burkhoff8, T. & Franz1, 9, and J. M. G., "Partial LVAD restores ventricular outputs and normalizes LV but not RV stress distributions in the acutely failing heart in silico." *Int J Artif Organs* 39, 421–430.

9. Bassingthwaighte, J. B., Chizeck, H. J. & Atlas, L. E., "Strategies and tactics in multiscale modeling of cell-to-organ systems." *Proc. IEEE* 94, 819–830 (2006).

10. Azevedo, P. S., Polegato, B. F., Minicucci, M. F., Paiva, S. A. R. & Zornoff, L. A. M., "Cardiac Remodeling: Concepts, Clinical Impact, Pathophysiological Mechanisms and Pharmacologic Treatment." *Arq. Bras. Cardiol.* 106, 62–69 (2016).

11. Shimkunas, R. *et al.,* "Left ventricular myocardial contractility is depressed in the borderzone after posterolateral myocardial infarction." *Ann. Thorac. Surg.* 95, 1619–1625 (2013).

12. Shavik, S. M., Wall, S. T., Sundnes, J., Burkhoff, D. & Lee, L. C., "Organ-level validation of a cross-bridge cycling descriptor in a left ventricular finite element model: Effects of ventricular loading on myocardial strains." *Physiol. Rep.* 5, 1–14 (2017).

13. Wenk, J. F. *et al.,* "Regional left ventricular myocardial contractility and stress in a finite element model of posterobasal myocardial infarction." *J. Biomech. Eng.* 133, (2011).

14. Shavik, S. M. *et al.,* "Computational Modeling Studies of the Roles of Left Ventricular Geometry, Afterload, and Muscle Contractility on Myocardial Strains in Heart Failure with Preserved Ejection Fraction." *J. Cardiovasc. Transl. Res.* 14, 1131–1145 (2021).

15. Triposkiadis, F. *et al.,* "Left ventricular geometry as a major determinant of left ventricular ejection fraction: physiological considerations and clinical implications." *Eur. J. Heart Fail.* 20, 436–444 (2018).

16. Aikawa, T. *et al.,* "Impaired left ventricular global longitudinal strain is associated with elevated left ventricular filling pressure after myocardial infarction." *Am. J. Physiol. - Hear. Circ. Physiol.* 319, 1474–1481 (2020).

17. Kasner, M., Sinning, D., Burkhoff, D. & Tschöpe, C., "Diastolic pressure–volume quotient (DPVQ) as a novel echocardiographic index for estimation of LV stiffness in HFpEF." *Clin. Res. Cardiol.* 104, 955–963 (2015).

18. Gorcsan, J. & Tanaka, H., "Echocardiographic assessment of myocardial strain." *J. Am. Coll.*

Cardiol. 58, 1401–1413 (2011).

19. Hirsch, G. A. *et al.,* "Age-related vascular stiffness and left ventricular size after myocardial infarction." *Am. J. Geriatr. Cardiol.* 16, 222–228 (2007).

20. Rajagopalan, V. *et al.,* "Safe oral triiodo-L-thyronine therapy protects from post-infarct cardiac dysfunction and arrhythmias without cardiovascular adverse effects." *PLoS One* 11, 1–16 (2016).

21. Elsman, P. *et al.,* "Impact of infarct location on left ventricular ejection fraction after correction for enzymatic infarct size in acute myocardial infarction treated with primary coronary intervention." *Am. Heart J.* 151, 1239.e9-1239.e14 (2006).

22. Yamamoto, K. *et al.,* "Myocardial stiffness is determined by ventricular fibrosis, but not by compensatory or excessive hypertrophy in hypertensive heart." *Cardiovasc. Res.* 55, 76–82 (2002).

23. Leong, C. O. *et al.,* "Computational Modelling of the Effect of Infarct Stiffness on Regional Myocardial Mechanics." *Proc. Annu. Int. Conf. IEEE Eng. Med. Biol. Soc. EMBS* 6952–6955 (2019) doi:10.1109/EMBC.2019.8856771.

24. McComb, C. *et al.,* "Assessment of the relationships between myocardial contractility and infarct tissue revealed by serial magnetic resonance imaging in patients with acute myocardial infarction." *Int. J. Cardiovasc. Imaging* 31, 1201–1209 (2015).